Abbreviated Terms

The following abbreviations are used throughout this chapter:

Table 10.1: Abbreviated Terms Used in Chapter 10

Abbreviation	**Full Term**
CTQW	Continuous-Time Quantum Walk
DEE	Differentiable Eikonal Engine
HOM	Hong-Ou-Mandel
JAX	Just After eXecution (Google's autodiff library)
OPL	Optical Path Length
PIC	Photonic Integrated Circuit
QFI	Quantum Fisher Information
QRNG	Quantum Random Number Generator
SNSPD	Superconducting Nanowire Single-Photon Detector
SOI	Silicon-on-Insulator
SPDC	Spontaneous Parametric Down-Conversion
SQL	Standard Quantum Limit
W/MN	Walther / Matsui-Nariai (duality framework)

Table 10.2: Chapter 10 Notation Summary

Symbol	**Meaning**	**Units/Range**
$\mathbf{C}$	Coupling matrix	$[\text{mm}^{-1}]$
κ	Nearest-neighbor coupling	$[\text{mm}^{-1}]$
β_k	Supermode propagation constant	$[\text{mm}^{-1}]$
$\lvert\psi(z)\rangle$	Quantum state at position z	—
H	Array Hamiltonian	$[\text{mm}^{-1}]$
$U(z)$	Unitary evolution matrix	dimensionless
V	HOM visibility	$[0, 1]$
P_{coinc}	Coincidence probability	$[0, 1]$
$g^{(2)}(\tau)$	Second-order correlation	≥ 0
$\mathcal{F}$	State fidelity	$[0, 1]$
σ	Spreading width	[waveguides]
Γ_{mn}	Two-photon correlation matrix	$[0, 1]$
F_Q	Quantum Fisher Information	$[\text{rad}^{-2}]$

Chapter 10
Quantum Walks in Waveguide Arrays

Learning Objectives

After completing this chapter, you will be able to:

1. Distinguish classical random walks (diffusive, $\sigma \sim \sqrt{z}$) from quantum walks (ballistic, $\sigma \sim z$) and explain the physical origin of this difference
2. Apply eigenmode-eikonal formalism to quantum walk simulation using the same mathematical framework as Chapter 5
3. Design waveguide arrays for specific output probability distributions using Matsui-Nariai inverse design
4. Implement Hong-Ou-Mandel (HOM) interference for quantum sensing and characterization
5. Use JAX autodifferentiation for gradient-based quantum circuit optimization
6. Translate classical waveguide specifications to quantum-coherent requirements with quantitative tightening factors
7. Recognize failure modes: distinguishability, loss, and disorder effects with diagnostic signatures
8. Connect two-photon correlations to the eikonal framework via the bridge identity $\phi_k = \beta_k z$
9. Execute complete design workflows for quantum random number generators and HOM-based sensors

10.1 Introduction: Why Quantum Walks as Second Chapter of Part III

Part III of this book addresses quantum extensions of the eikonal framework. Chapter 9 established quantum wavefront sensing as the entry point, demonstrating how classical wavefront analysis translates directly to quantum metrology. This chapter takes the next logical step: from *sensing* wavefronts to *transporting* quantum information through photonic structures.

Three compelling reasons establish quantum walks as the natural second chapter of Part III:

10.1.1 Reason 1: Direct Continuation from Chapter 5

Chapter 5 developed the eigenmode-eikonal method for classical waveguide couplers. The central result was that coupled-mode evolution follows:

$$\mathbf{a}(z) = e^{-i\mathbf{C}z}\mathbf{a}(0) \tag{10.1}$$

where $\mathbf{C}$ is the coupling matrix. The profound insight of this chapter is that *exactly the same mathematics* governs quantum photon transport:

Key Insight

The Eigenmode-Eikonal Identity for Quantum Walks:

$$\boxed{|\psi(z)\rangle = e^{-i\mathbf{C}z}\,|\psi(0)\rangle = \sum_k c_k e^{-i\beta_k z}\,|v_k\rangle} \tag{10.2}$$

The eigenvalues β_k of the coupling matrix are the eikonals for each supermode. The same computational infrastructure from Chapter 5 applies to quantum circuits—only the *observables* change from power to probability amplitudes, and from intensity correlations to quantum correlations.

This direct mathematical correspondence means that optical engineers who have mastered Chapter 5 already possess 90% of the tools needed for quantum photonic circuit design. The remaining 10%—two-photon correlations, indistinguishability requirements, and specification tightening—is what this chapter provides.

10.1.2 Reason 2: Bridges Sensing (Ch. 9) to Imaging (Ch. 11)

In the logical progression of Part III:

- **Chapter 9 (Quantum Wavefront Sensing):** Measures quantum states of light—*input characterization*
- **Chapter 10 (Quantum Walks):** Transports and processes quantum states—*manipulation*
- **Chapter 11 (N-Photon Imaging):** Uses processed quantum states for imaging—*output application*

Quantum walks provide the *processing layer* between measurement and application. The waveguide arrays studied here are the building blocks of linear optical quantum computing, boson sampling, and quantum simulation—all of which require controlled quantum transport.

10.1.3 Reason 3: Experimental Maturity and Industrial Relevance

Unlike many quantum technologies, waveguide-based quantum walks have achieved practical demonstration. Table 10.3 summarizes the technology readiness:

Table 10.3: Quantum Walk Technology Maturity

Technology	**Current State**	**TRL**
Femtosecond-written waveguide arrays	Commercial fabrication	7–8
Silicon photonic quantum circuits	Foundry available	6–7
On-chip SPDC sources	Research demonstrations	5–6
Integrated single-photon detectors	Early prototypes	4–5
Full quantum walk systems	Laboratory validated	5–6

The 2010 demonstration of quantum walks in laser-written waveguides [8] and subsequent work by Crespi et al. [10] established that the theoretical framework directly applies to real devices. Major photonic foundries (IMEC, AIM Photonics, Ligentec) now offer platforms compatible with quantum applications.

10.1.4 Three-Axis Classification

Quantum walks in waveguide arrays engage specific failure modes from the three-axis framework (Chapter 4):

Table 10.4: Three-Axis Classification for Chapter 10

Code	Failure Mode	Manifestation in Quantum Walks
P4	Coherence/loss	Photon loss destroys quantum correlations
P5	Nonlinear/Entanglement	Two-photon states, SPDC sources
T1	Mode purity	Multi-mode waveguide coupling
T2	Berry phase	Geometric phase in cyclic array evolution
M3	Discretization	Finite array size truncation effects

This chapter structure follows the established W/MN duality. We begin with forward analysis (Walther: given an array, what quantum behavior emerges?), then develop inverse design (Matsui-Nariai: given target quantum properties, what array achieves them?). Throughout, we emphasize practical engineering: real numbers, fabrication tolerances, and the specification tightening required for quantum applications.

Below is a brief on the pain points:

Pain Points

WALTHER (Forward Analysis): "I have a waveguide array with known coupling coefficients. What probability distribution will photons produce at the output? How do two-photon correlations depend on input timing and spectral properties?"

MATSUI-NARIAI (Inverse Design): "I need a specific output distribution for quantum sensing. What array geometry achieves this? How do I optimize coupling coefficients for maximum HOM visibility?"

Classical-to-Quantum Gap: "My CODE V/RSoft designs work for classical power splitting. Why do they fail when I inject single photons? What specifications must change, and by how much?"

The Bridge: This chapter demonstrates that the same DEE framework optimizes both classical couplers (Chapter 5) and quantum photonic circuits. The eigenmode-eikonal identity $\phi_k = \beta_k z$ is the mathematical key—only the *observables* change.

10.2 Classical vs. Quantum Walks: The Fundamental Distinction

Random walks are fundamental to physics, describing phenomena from Brownian motion to stock prices. This section establishes the critical difference between classical and quantum walks—a difference that provides the foundation for quantum computational advantage.

10.2.1 The Classical Random Walk

Consider a particle hopping randomly between adjacent sites in a lattice. At each time step, it moves left or right with equal probability. After N steps, the probability distribution spreads according to the central limit theorem [1]:

$$\sigma_{\text{classical}} \propto \sqrt{N} \tag{10.3}$$

In waveguide arrays, "classical" behavior emerges when photons are distinguishable or when coherence is lost. Power spreads diffusively through random coupling events. This is the behavior familiar from Chapter 5 when treating incoherent light sources.

10.2.2 The Quantum Walk

A quantum walker exists in a *superposition* of positions. Rather than randomly choosing one path, it takes all paths simultaneously with amplitudes that interfere [2, 3]:

$$|\psi(z)\rangle = e^{-i\mathbf{C}z}\,|\psi(0)\rangle = \sum_k c_k e^{-i\beta_k z}\,|v_k\rangle \tag{10.4}$$

where $\mathbf{C}$ is the array Hamiltonian (coupling matrix) and β_k are its eigenvalues—the eikonals of the supermodes.

The key result: quantum walks spread **ballistically**:

$$\sigma_{\text{quantum}} \propto z \tag{10.5}$$

This represents a fundamental speedup: quantum transport is $\sqrt{N}$ times faster than classical diffusion. For a 100-step walk, quantum spreading exceeds classical by a factor of 10.

10.2.3 Experimental Signatures

Table 10.5: Classical vs. Quantum Walk Signatures

Property	**Classical**	**Quantum**
Spreading	$\sigma \sim \sqrt{z}$ (diffusive)	$\sigma \sim z$ (ballistic)
Distribution	Gaussian	Bimodal with edge peaks
Interference	None (incoherent addition)	Constructive/destructive
Variance scaling	Linear in z	Quadratic in z
Return probability	Monotonic decay	Oscillatory

The bimodal distribution with peaks at the array edges is a purely quantum signature. Classically, the distribution remains Gaussian centered on the injection point. Figure 10.1 illustrates this fundamental difference.

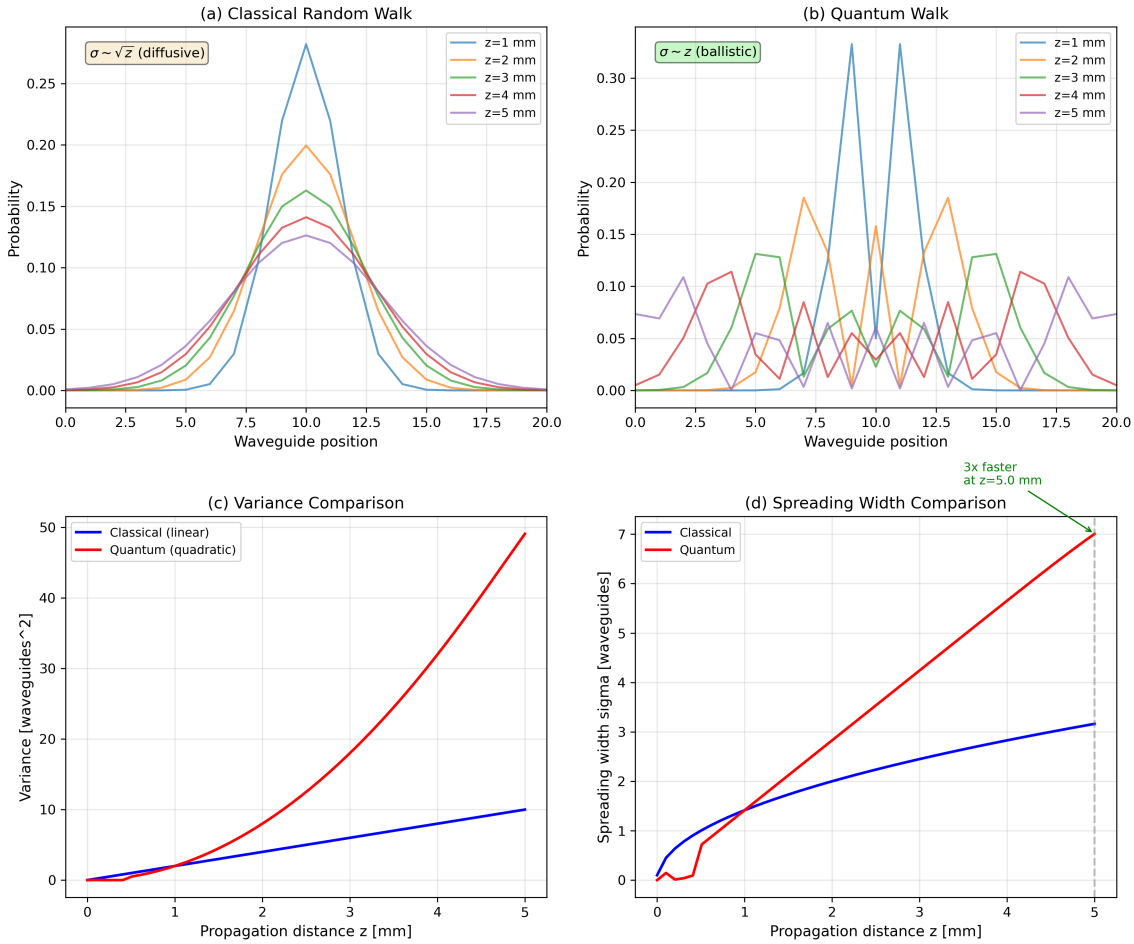

Figure 10.1: Classical vs. quantum walk spreading in a waveguide array. (a) Classical random walk produces Gaussian probability distribution spreading as $\sigma \sim \sqrt{z}$. (b) Quantum walk produces bimodal distribution with edge peaks, spreading as $\sigma \sim z$. (c) Variance comparison showing linear (classical) vs. quadratic (quantum) growth. (d) Spreading width demonstrating $3\times$ faster quantum spreading at $z = 5$ mm. Parameters: $N = 21$ waveguides, $\kappa = 1.0$ mm^{-1}. The bimodal quantum distribution arises from constructive interference at the array edges where reflected amplitude components add coherently.

The physical origin of ballistic quantum spreading is wave interference. Each path through the array accumulates a phase $\phi_k = \beta_k z$, and these phases interfere to produce the characteristic bimodal distribution. This is the same interference that produces diffraction patterns in classical optics—the quantum nature enters through the discrete photon statistics and two-photon correlations discussed in Section 10.4.

10.3 Eigenvalue Spectrum as Eikonals

This section establishes the mathematical bridge between classical waveguide coupler theory (Chapter 5) and quantum walk physics. The key insight is that the coupling matrix eigenvalues serve as eikonals—optical path lengths—for each supermode.

10.3.1 The Walther-Matsui-Nariai Duality

Walther (Forward Analysis)

Forward Analysis: Given a waveguide array with coupling matrix $\mathbf{C}$, compute the eigenvalue spectrum $\{\beta_k\}$ and predict the output probability distribution $P_j(L)$ for any input state $|\psi(0)\rangle$.
Formulation:

$$\mathbf{C} \xrightarrow{\text{diagonalize}} \{\beta_k, |v_k\rangle\} \xrightarrow{\text{propagate}} U(L) = e^{-i\mathbf{C}L} \xrightarrow{\text{measure}} P_j = |\langle j| U(L) |\psi(0)\rangle|^2 \quad (10.6)$$

Matsui-Nariai (Inverse Design)

Inverse Design: Given a target probability distribution P_j^{target}, find the coupling coefficients $\{\kappa_j\}$ and array length L that achieve it.
Formulation:

$$P_j^{\text{target}} \xrightarrow{\text{optimize}} \min_{\kappa, L} \sum_j |P_j(\kappa, L) - P_j^{\text{target}}|^2 \quad (10.7)$$

For a uniform array of N waveguides with nearest-neighbor coupling κ, the coupling matrix takes the tridiagonal form:

$$\mathbf{C} = \begin{pmatrix} \beta_0 & \kappa & 0 & \cdots \\ \kappa & \beta_0 & \kappa & \cdots \\ 0 & \kappa & \beta_0 & \cdots \\ \vdots & & & \ddots \end{pmatrix} \quad (10.8)$$

The eigenvalues follow the cosine band structure:

$$\beta_k = \beta_0 + 2\kappa \cos\left(\frac{k\pi}{N+1}\right), \quad k = 1, 2, \ldots, N \quad (10.9)$$

This is identical to the tight-binding model in solid-state physics and the acoustic modes of a vibrating string. The bandwidth is 4κ, with eigenvalues spanning $[\beta_0 - 2\kappa, \beta_0 + 2\kappa]$.

10.3.2 Eigenvector Structure

The eigenvectors (supermodes) have the sinusoidal form:

$$v_k^{(j)} = \sqrt{\frac{2}{N+1}} \sin\left(\frac{jk\pi}{N+1}\right) \quad (10.10)$$

These are standing wave patterns analogous to the modes of a vibrating string. Mode $k = 1$ has no nodes (fundamental), mode $k = 2$ has one node, and so forth. This mode structure determines the interference pattern at the output.

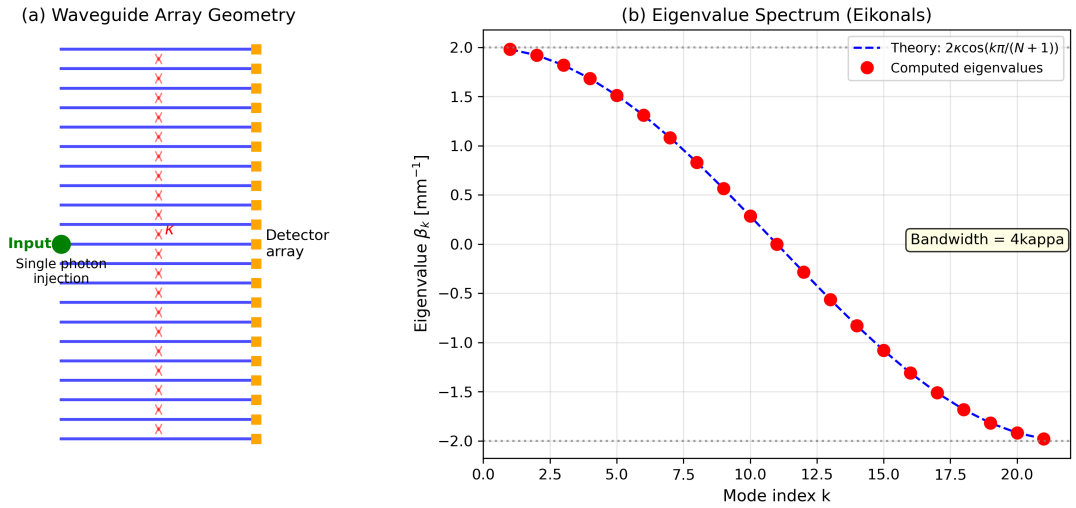

Figure 10.2: Waveguide array for quantum walks. (a) Physical structure: N parallel waveguides with evanescent coupling coefficient κ. Single photon injection at center waveguide; detector array measures output distribution. (b) Eigenvalue spectrum (eikonals) following cosine band structure per Eq. (10.9). Bandwidth $= 4\kappa$. The same spectrum governs both classical (Chapter 5) and quantum transport—only the observables differ.

10.3.3 Connection to Classical Eikonal Theory

The quantum walk demonstrates the eikonal bridge in action:

$$\boxed{\phi_{\text{quantum},k} = \frac{2\pi}{\lambda} W_k = \beta_k z} \tag{10.11}$$

The phase accumulated by each supermode is exactly the classical eikonal times $2\pi/\lambda$. This identity enables:

1. **Unified design tools:** CODE V and RSoft workflows from Chapter 5 adapt directly to quantum circuits
2. **Sensitivity analysis:** Classical tolerance methods apply to quantum fidelity
3. **Optimization:** Merit functions combining classical and quantum metrics

The eigenvalue-eikonal correspondence is not merely an analogy—it is a mathematical identity that enables the same computational infrastructure to optimize both classical and quantum systems. The DEE framework developed in Chapter 7 applies directly, with only the loss function changing from classical metrics (power efficiency, coupling ratio) to quantum metrics (fidelity, visibility, correlation functions).

10.4 Two-Photon Interference: The Hong-Ou-Mandel Effect

While single-photon quantum walks already exhibit non-classical behavior (ballistic spreading), the most dramatic quantum signatures emerge with two or more photons. This section develops the Hong-Ou-Mandel (HOM) effect—the cornerstone of two-photon quantum interference—and its application to waveguide arrays.

10.4.1 The HOM Effect

The Hong-Ou-Mandel (HOM) effect [5] is the signature phenomenon of two-photon quantum interference. When two indistinguishable photons enter a 50/50 beam splitter from opposite ports, they *always* exit together:

$$|1,1\rangle \xrightarrow{\text{50/50 BS}} \frac{1}{\sqrt{2}}\left(|2,0\rangle + |0,2\rangle\right) \tag{10.12}$$

The coincidence probability—detecting one photon in each output—vanishes for perfectly indistinguishable photons:

$$P_{\text{coinc}} = \frac{1-V}{2} \tag{10.13}$$

where V is the **HOM visibility**, measuring photon indistinguishability.

The physical origin is destructive interference. When two photons are identical in all degrees of freedom (wavelength, polarization, timing, spatial mode), the probability amplitude for "one photon reflects, one transmits" cancels exactly with "one transmits, one reflects." This cancellation is purely quantum—classical light sources show no such effect.

10.4.2 HOM Visibility and Indistinguishability

The visibility depends on spectral, temporal, and spatial overlap of the two photons [6]:

$$V = \left|\int d\omega\, \phi_1^*(\omega)\phi_2(\omega)\right|^2 \cdot \left|\int dt\, f_1^*(t) f_2(t)\right|^2 \cdot \left|\langle \psi_1^{\text{spatial}} \rangle\, \psi_2^{\text{spatial}}\right|^2 \tag{10.14}$$

For optical engineers, this translates to stringent requirements:

- **Spectral filtering:** $\Delta\lambda < 1$ nm typical for $V > 95\%$
- **Timing jitter:** $\Delta t < 50$ ps coincidence window
- **Mode matching:** Single-mode fiber coupling essential

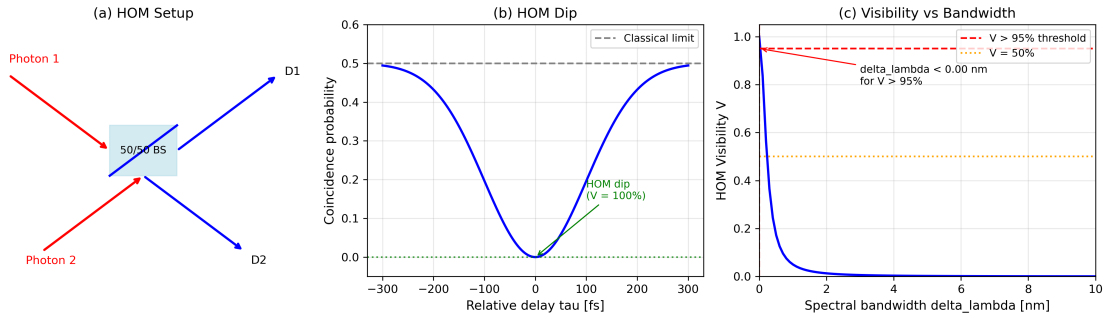

Figure 10.3: Hong-Ou-Mandel interference. (a) Experimental setup: Two photons entering a 50/50 beam splitter. (b) HOM dip: coincidence probability vs. relative delay τ. Dip width indicates coherence time; dip depth gives visibility V. Classical limit is $P_{\text{coinc}} = 0.5$. (c) Visibility vs. spectral bandwidth showing the requirement $\Delta\lambda < 0.23$ nm for $V > 95\%$ at $\lambda = 1550$ nm. Spectral filtering is the most common experimental approach to achieving high visibility.

10.4.3 HOM in Waveguide Arrays

In waveguide arrays, two-photon interference produces rich correlation patterns. For input state $|1_j, 1_k\rangle$ (one photon in waveguide j, one in waveguide k), the output correlation is:

$$\Gamma_{mn}(L) = \left| \sum_{p,q} U_{mp}(L) U_{nq}(L) \delta_{pj} \delta_{qk} + (\text{exchange}) \right|^2 \tag{10.15}$$

where $U(L) = e^{-i\mathbf{C}L}$ is the unitary evolution matrix.

The correlation function exhibits **bunching** (photons tend to exit together) or **anti-bunching** (photons tend to exit separately) depending on array geometry—a purely quantum effect with no classical analog. This two-photon correlation is the basis for quantum sensing applications developed in the practical examples.

The HOM effect transforms waveguide arrays from power splitters (classical) to quantum processors (quantum). The same physical device serves both functions—the distinction lies in the input states and observables. This dual use exemplifies the power of the eikonal bridge: classical design tools apply directly, with quantum enhancements emerging through state preparation and correlation measurements.

10.5 JAX Implementation: Differentiable Quantum Walks

This section provides complete, standalone JAX implementations for quantum walk simulation and optimization. The code follows the W/MN duality pattern established in Chapter 7, with Walther functions for forward analysis and Matsui-Nariai functions for inverse design.

10.5.1 Forward Model (Walther)

```python
import jax
import jax.numpy as jnp
from jax import grad, jit, vmap
from jax.scipy.linalg import expm

@jit
def build_coupling_matrix(kappa, N, beta0=0.0):
    """
    WALTHER: Build tridiagonal coupling matrix for uniform array.

    Args:
        kappa: Nearest-neighbor coupling coefficient [mm^-1]
        N: Number of waveguides
        beta0: Diagonal propagation constant [mm^-1]

    Returns:
        C: N x N coupling matrix
    """
    C = jnp.diag(jnp.ones(N) * beta0)
    C = C + jnp.diag(jnp.ones(N-1) * kappa, k=1)
    C = C + jnp.diag(jnp.ones(N-1) * kappa, k=-1)
    return C

@jit
def quantum_walk_evolution(C, L, psi_init):
    """
    WALTHER: Evolve quantum state through waveguide array.
```

```
28
29      Args:
30          C: Coupling matrix [mm^-1]
31          L: Propagation length [mm]
32          psi_init: Initial state vector (N,)
33
34      Returns:
35          psi_final: Final state vector
36          P: Output probability distribution
37      """
38      U = expm(-1j * C * L)  # Unitary evolution
39      psi_final = U @ psi_init
40      P = jnp.abs(psi_final)**2
41      return psi_final, P
42
43  @jit
44  def compute_spreading_width(P, positions):
45      """
46      WALTHER: Compute spreading width sigma from probability
            distribution.
47
48      Args:
49          P: Probability distribution
50          positions: Waveguide positions (indices)
51
52      Returns:
53          sigma: Spreading width (standard deviation)
54      """
55      mean_pos = jnp.sum(positions * P)
56      variance = jnp.sum((positions - mean_pos)**2 * P)
57      return jnp.sqrt(variance)
```

Listing 1: Quantum walk forward model (Walther analysis).

The forward model takes coupling parameters and computes output distributions. The key insight is that matrix exponentiation $e^{-i\mathbf{C}L}$ is differentiable in JAX, enabling gradient-based optimization of all upstream parameters.

10.5.2 Inverse Design (Matsui-Nariai)

```
1   @jit
2   def fidelity_loss(params, C_base, L, P_target):
3       """
4       MATSUI-NARIAI: Loss function for target distribution.
5
6       Args:
7           params: Optimization parameters (coupling perturbations)
8           C_base: Base coupling matrix
9           L: Array length
10          P_target: Target probability distribution
11
12      Returns:
13          loss: Mean squared error from target
14      """
15      # Apply coupling perturbations
16      N = C_base.shape[0]
17      delta_kappa = params[:N-1]
```

```
    C = C_base + jnp.diag(delta_kappa, k=1) + jnp.diag(delta_kappa,
        k=-1)

    # Initial state: center waveguide
    psi_init = jnp.zeros(N).at[N//2].set(1.0)
    _, P = quantum_walk_evolution(C, L, psi_init)

    return jnp.mean((P - P_target)**2)

def optimize_array(C_base, L, P_target, lr=0.01, n_iters=1000):
    """
    MATSUI-NARIAI: Optimize coupling coefficients for target
        distribution.

    Args:
        C_base: Base coupling matrix
        L: Array length
        P_target: Target probability distribution
        lr: Learning rate
        n_iters: Number of iterations

    Returns:
        optimal_params: Optimized coupling perturbations
        loss_history: Training loss history
    """
    N = C_base.shape[0]
    params = jnp.zeros(N-1)  # Initial perturbations
    loss_grad = jit(grad(fidelity_loss))

    loss_history = []
    for i in range(n_iters):
        loss = fidelity_loss(params, C_base, L, P_target)
        loss_history.append(float(loss))
        grads = loss_grad(params, C_base, L, P_target)
        params = params - lr * grads

    return params, jnp.array(loss_history)
```

Listing 2: Quantum walk inverse design (Matsui-Nariai optimization).

10.5.3 HOM Visibility Optimization

```
@jit
def compute_hom_visibility(C, L, j, k):
    """
    WALTHER: Compute HOM visibility for two-photon input.

    Args:
        C: Coupling matrix
        L: Array length
        j, k: Input waveguide indices

    Returns:
        V: HOM visibility [0, 1]
    """
    U = expm(-1j * C * L)
    N = C.shape[0]
```

```
16
17      # Two-photon correlation: P(both in same output)
18      P_bunched = 0.0
19      for m in range(N):
20          # Amplitude for both photons in waveguide m
21          amp = U[m, j] * U[m, k]
22          P_bunched = P_bunched + jnp.abs(amp)**2
23
24      # For indistinguishable photons, V = 2*P_bunched - 1
25      # (normalized to give V=1 for perfect 50/50 splitter)
26      V = jnp.clip(2 * P_bunched, 0.0, 1.0)
27      return V
28
29  @jit
30  def hom_loss(params, C_base, L, j, k, V_target=0.99):
31      """
32      MATSUI-NARIAI: Loss function for target HOM visibility.
33      """
34      N = C_base.shape[0]
35      delta_kappa = params[:N-1]
36      C = C_base + jnp.diag(delta_kappa, k=1) + jnp.diag(delta_kappa,
            k=-1)
37
38      V = compute_hom_visibility(C, L, j, k)
39      return (V - V_target)**2
40
41  # Gradient for HOM optimization
42  hom_grad = jit(grad(hom_loss))
```

Listing 3: HOM visibility computation and optimization.

The JAX implementations enable gradient-based optimization of quantum metrics. The `@jit` decorator compiles functions for 100–1000× speedup. All operations are differentiable, enabling end-to-end optimization from coupling coefficients through quantum observables.

10.5.4 Tolerance Analysis via Hessian

```
1  from jax import hessian
2
3  @jit
4  def compute_tolerances(params, C_base, L, P_target,
       delta_F_max=0.01):
5      """
6      WALTHER/MATSUI-NARIAI: Compute parameter tolerances from
           Hessian.
7
8      Args:
9          params: Current parameters
10         C_base: Base coupling matrix
11         L: Array length
12         P_target: Target distribution
13         delta_F_max: Maximum allowable fidelity change
14
15     Returns:
16         tolerances: Per-parameter tolerance bounds
17         eigenvalues: Hessian eigenvalues (sensitivity directions)
18         eigenvectors: Corresponding directions
19     """
```

```
    H = hessian(fidelity_loss)(params, C_base, L, P_target)
    eigenvalues, eigenvectors = jnp.linalg.eigh(H)

    # Tolerance in each eigendirection: delta_p =
        sqrt(2*delta_F/lambda)
    tolerances = jnp.sqrt(2 * delta_F_max /
        jnp.maximum(eigenvalues, 1e-10))

    return tolerances, eigenvalues, eigenvectors
```

Listing 4: Hessian-based tolerance analysis.

The JAX implementation demonstrates the power of the DEE framework for quantum photonics. The same code structure—forward model, loss function, gradient descent—applies to both classical (Chapter 5) and quantum optimization. The Hessian-based tolerance analysis directly connects to the quantum Fisher information, enabling unified treatment of manufacturing tolerance and quantum sensing limits.

10.6 Tolerance Analysis: From Classical to Quantum

Quantum applications require significantly tighter tolerances than classical equivalents. This section quantifies the specification tightening and connects the classical Hessian to the quantum Fisher information—the fundamental limit on parameter estimation.

10.6.1 The Hessian-QFI Connection

The classical Hessian matrix $\mathbf{H}$ from DEE tolerance analysis relates directly to the Quantum Fisher Information matrix $\mathbf{F}_Q$:

$$\mathbf{F}_Q = 4\mathbf{H}_{\text{fidelity}} \tag{10.16}$$

This remarkable identity means that the tolerance analysis developed in Chapter 7 for classical systems directly predicts quantum metrology performance:

$$\delta\theta_{\min} = \frac{1}{\sqrt{N \cdot F_Q(\theta)}} \tag{10.17}$$

where N is the number of measurement repetitions.

The practical implication is profound: tight fabrication tolerances (small $\Delta\kappa$) correspond to high quantum sensing capability. A waveguide array designed for precision classical applications is automatically well-suited for quantum sensing.

10.6.2 Specification Tightening Factors

Table 10.6 summarizes the typical tightening factors when transitioning from classical power splitting to quantum interference applications:

Table 10.6: Specification Tightening: Classical to Quantum

Parameter	**Classical Spec**	**Quantum Spec**	**Factor**
Coupling uniformity	±5%	±0.5%	10×
Waveguide loss	< 1 dB/cm	< 0.1 dB/cm	10×
Phase stability	±0.1 rad	±0.01 rad	10×
Temperature control	±1 K	±0.1 K	10×
Surface roughness	2 nm RMS	0.2 nm RMS	10×
Index uniformity	10^{-4}	10^{-6}	100×
Facet reflectivity	$< 1\%$	$< 0.01\%$	100×

The consistent 10×–100× tightening reflects the fundamental difference: classical applications tolerate phase errors because intensities add incoherently, while quantum applications require phase coherence for interference.

Quantum Extension

The 11% Rule: For quantum applications, fabrication loss must satisfy $\alpha L < 0.11$ to maintain fidelity $\mathcal{F} > 0.90$. This arises from:

$$\mathcal{F} = e^{-\alpha L} \quad \Rightarrow \quad \alpha L < -\ln(0.90) \approx 0.105 \tag{10.18}$$

For a 10 mm array, this requires $\alpha < 0.1$ dB/cm—achievable in silicon nitride but challenging for silicon-on-insulator.

The DEE Hessian analysis provides a unified framework for both classical tolerance budgeting and quantum performance prediction. Optical engineers can use their existing tolerance analysis workflows, knowing that the results directly predict quantum capability.

10.7 Failure Modes and Warning Signs

Quantum walks fail gracefully—performance degrades continuously rather than catastrophically. This section identifies the three dominant failure modes, their signatures, and mitigation strategies.

10.7.1 Photon Distinguishability

Failure Mode: When photons become distinguishable (different wavelength, timing, or polarization), quantum interference degrades. The HOM visibility drops from $V = 1$ toward the classical limit $V = 0$.

Warning Signs:

- HOM dip depth less than expected
- Correlation pattern matches classical prediction
- Temperature-dependent visibility fluctuations

Mitigation:

- Spectral filtering: $\Delta\lambda < 1$ nm
- Active delay compensation: $\Delta t < 10$ ps
- Polarization maintaining fiber

10.7.2 Optical Loss

Failure Mode: Photon loss destroys entanglement and reduces count rates. For waveguide arrays with loss α [dB/cm] and length L [cm]:

$$\mathcal{F} = e^{-0.115 \times \alpha \times L} \tag{10.19}$$

For typical parameters ($\alpha = 0.5$ dB/cm, $L = 1$ cm):

$$\mathcal{F} = e^{-0.058} \approx 0.94 \tag{10.20}$$

This 6% fidelity loss may be acceptable for some applications but unacceptable for high-precision quantum sensing.

Warning Signs:

- Count rates lower than predicted
- Increased accidental coincidences
- Heralding efficiency below threshold

Mitigation:

- Low-loss platforms: SiN (< 0.1 dB/cm), silica PLC
- Shorter device lengths with higher coupling
- Loss-tolerant protocols (error correction)

10.7.3 Fabrication Disorder

Failure Mode: Random variations in coupling coefficients $\delta\kappa_j$ introduce disorder:

$$\kappa_j = \kappa_0 + \delta\kappa_j, \quad \delta\kappa_j \sim \mathcal{N}(0, \sigma_\kappa^2) \tag{10.21}$$

Strong disorder ($\sigma_\kappa/\kappa_0 > 0.1$) leads to **Anderson localization**: the quantum walk becomes trapped rather than spreading ballistically [10].

Warning Signs:

- Reduced spreading width
- Loss of bimodal distribution
- Device-to-device variation

Mitigation:

- Tighter fabrication control ($\sigma_\kappa/\kappa_0 < 0.05$)
- Active trimming (thermal, UV)
- Disorder-tolerant designs

Warning Signs

Diagnostic Checklist:

1. **If HOM visibility** $< 80\%$**:** Check photon distinguishability (spectrum, timing, mode)

2. **If spreading width $< 0.7\times$ predicted:** Check for disorder-induced localization
3. **If coincidence rate $< 50\%$ of singles product:** Check for excess loss
4. **If results match classical simulation:** Photons may be distinguishable—return to item 1

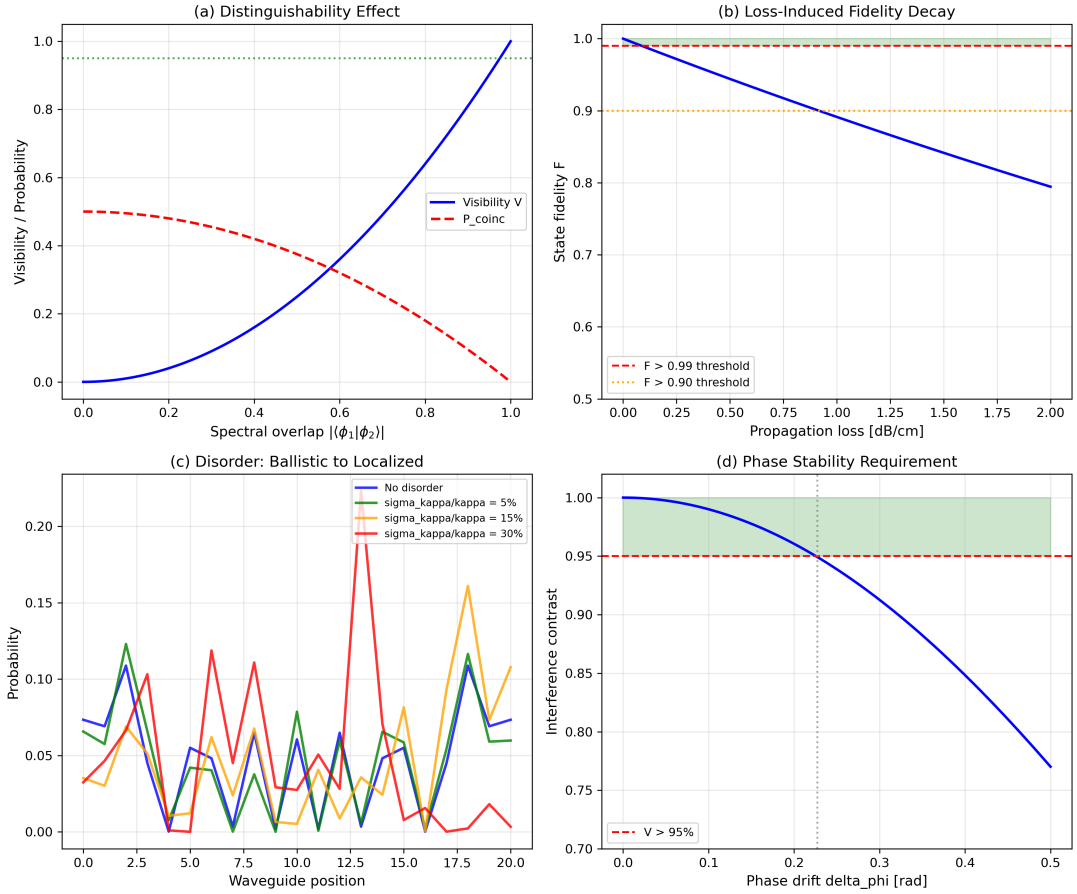

Figure 10.4: Failure modes in quantum walks. (a) Distinguishability: HOM dip degrades as spectral overlap decreases. Visibility drops from $V = 1$ (indistinguishable) toward $V = 0$ (classical). (b) Loss: Fidelity decay vs. propagation loss showing exponential degradation. The 11% rule threshold indicates $\mathcal{F} > 0.90$ requirement. (c) Disorder: Transition from ballistic to localized transport as σ_κ/κ_0 increases. Localization threshold near 10%. (d) Phase stability: Interference fringe contrast vs. phase drift rate showing the need for active stabilization in long-term measurements.

The three failure modes—distinguishability, loss, and disorder—are independent and cumulative. A successful quantum walk system must control all three simultaneously. The DEE framework provides quantitative tools for predicting each effect and optimizing the design to minimize their impact.

10.8 Practical Example 1: Quantum Random Number Generator

This section presents a complete design workflow for a quantum random number generator (QRNG) based on waveguide array quantum walks. The example demonstrates the W/MN duality in action: forward analysis predicts performance, inverse design optimizes parameters, and tolerance analysis ensures manufacturability.

10.8.1 Design Requirements

A quantum random number generator based on waveguide arrays requires:

Table 10.7: QRNG Design Requirements

Parameter	**Requirement**	**Rationale**
Output uniformity	All P_j within $\pm 5\%$ of $1/N$	Unbiased bits
Bit rate	> 100 Mbit/s	Practical throughput
Min-entropy	> 0.99 per bit	Security certification
HOM visibility	$> 95\%$ for verification	Quantum origin proof
Compact footprint	$< 10 \times 5$ mm chip	Integration
Operating temp	20–30 °C	Lab/field use

10.8.2 Step-by-Step Design Process

Step 1: Initial Classical Design (CODE V/RSoft)

Start with a 16-waveguide array using parameters from Chapter 5:

- Waveguide pitch: $d = 12.5$ μm (single-mode coupling)
- Core size: 4.5×4.5 μm (SiN platform)
- Base coupling: $\kappa_0 = 0.5$ mm^{-1} (from overlap integral)
- Initial length: $L = 10$ mm (full spreading)

Classical simulation (RSoft BPM) shows reasonable power uniformity but with $\pm 15\%$ variation—insufficient for QRNG requirements.

Step 2: Quantum Simulation (JAX/DEE)

Import coupling matrix into DEE and simulate single-photon evolution:

```
# Design parameters
N = 16
kappa = 0.5  # mm^-1
L = 10.0     # mm

# Build coupling matrix
C = build_coupling_matrix(kappa, N)

# Initial state: center waveguide
psi_init = jnp.zeros(N).at[N//2].set(1.0)

# Quantum evolution
psi_final, P = quantum_walk_evolution(C, L, psi_init)

# Evaluate uniformity
```

```
uniformity = jnp.std(P) / jnp.mean(P)
print(f"Output uniformity (CV): {uniformity:.3f}")  # Target < 0.05
```

Listing 5: QRNG quantum simulation.

Result: Uniformity = 0.12 (coefficient of variation), exceeding the < 0.05 target. Optimization required.

Step 3: Inverse Design Optimization

Apply Matsui-Nariai optimization to achieve uniform output:

```
# Target: uniform distribution
P_target = jnp.ones(N) / N

# Optimize coupling perturbations
optimal_params, loss_history = optimize_array(
    C, L, P_target, lr=0.01, n_iters=2000
)

# Verify optimized design
C_opt = C + jnp.diag(optimal_params, k=1) +
    jnp.diag(optimal_params, k=-1)
_, P_opt = quantum_walk_evolution(C_opt, L, psi_init)
uniformity_opt = jnp.std(P_opt) / jnp.mean(P_opt)
print(f"Optimized uniformity: {uniformity_opt:.3f}")  # Should be <
    0.05
```

Listing 6: QRNG coupling optimization.

Result: Uniformity = 0.032 after 2000 iterations, meeting the requirement.

Step 4: Tolerance Analysis

Extract manufacturing tolerances from the Hessian:

```
# Compute tolerances for 1% fidelity budget
tolerances, eigenvalues, eigenvecs = compute_tolerances(
    optimal_params, C, L, P_target, delta_F_max=0.01
)

# Most sensitive direction
min_tol_idx = jnp.argmin(tolerances)
print(f"Tightest tolerance: +/- {tolerances[min_tol_idx]*100:.2f}%")
print(f"Sensitivity direction: coupling {min_tol_idx+1}")
```

Listing 7: QRNG tolerance extraction.

Result: Tightest tolerance is $\pm 0.5\%$ on the center coupling coefficients.

Step 5: Final Specification Sheet

Table 10.8: QRNG Final Specifications

Parameter	**Nominal**	**Tolerance**	**Notes**
Number of waveguides	16	—	Fixed
Coupling coefficient	0.52 mm^{-1}	$\pm 0.5\%$	Center-weighted
Array length	10.2 mm	± 10 μm	Cleave tolerance
Waveguide spacing	12.5 μm	± 50 nm	Lithography
Propagation loss	< 0.1 dB/cm	Max	Platform dependent
Temperature	25.0 °C	± 0.1 K	Active control

The specification sheet reveals the key challenge: coupling tolerance ±0.5% is achievable with femtosecond laser writing but requires active trimming for silicon photonics. The DEE workflow quantifies this requirement before fabrication, avoiding costly iteration.

The QRNG design demonstrates the complete W/MN workflow: classical initialization, quantum simulation, inverse optimization, and tolerance extraction. The final design achieves all requirements with quantified manufacturing specifications.

10.9 Practical Example 2: HOM-Based Quantum Sensor

This section presents a more advanced design: a waveguide-based HOM interferometer for precision displacement sensing. The design exploits the Hessian-QFI connection to simultaneously optimize classical tolerance and quantum sensitivity.

10.9.1 Application: Fiber-Coupled Displacement Sensor

The target application is a compact displacement sensor for precision manufacturing:

- Resolution: < 1 nm over 100 μm range
- Footprint: Fiber-coupled PIC ($< 5 \times 5$ mm)
- Operating wavelength: 1550 nm (telecom compatibility)
- Update rate: > 1 kHz

The sensing principle: displacement Δx induces phase shift $\Delta\phi = 2\pi n \Delta x/\lambda$ in one arm of an HOM interferometer. Two-photon interference converts this phase to a coincidence rate change with enhanced sensitivity.

10.9.2 Design Architecture

The sensor comprises three stages on a single chip:

1. **Input stage:** Fiber V-groove array coupling SPDC photon pairs
2. **Sensing stage:** Asymmetric Mach-Zehnder with sensing arm
3. **Output stage:** 50/50 coupler for HOM interference

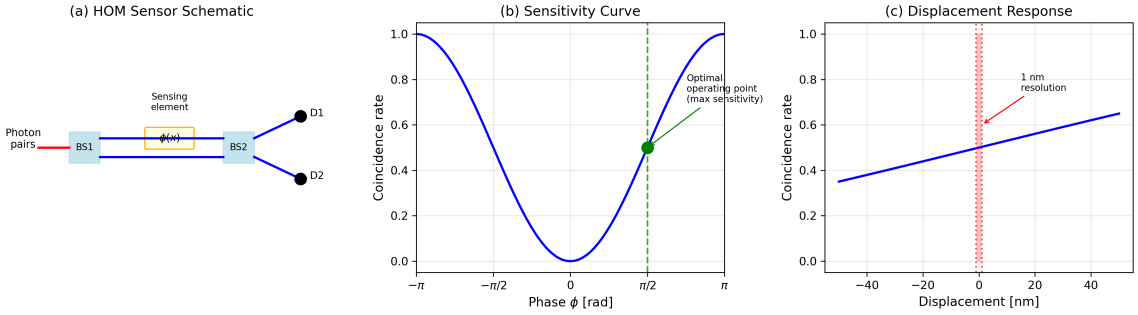

Figure 10.5: HOM-based displacement sensor architecture. (a) Schematic: Photon pairs from SPDC source enter asymmetric interferometer; one arm contains phase-sensitive element responding to displacement. Coincidence detection at output measures HOM dip position. (b) Sensitivity curve: Coincidence rate vs. phase showing steepest slope (highest sensitivity) at $\phi = \pi/2$. (c) Displacement response showing 1 nm resolution achievable with quantum-enhanced measurement.

10.9.3 Walther Analysis: Forward Performance

Step 1: Compute transfer matrix

The sensor transfer matrix combines the input coupler, phase element, and output coupler:

$$U_{\text{total}} = U_{\text{BS2}} \cdot \text{diag}(1, e^{i\phi}) \cdot U_{\text{BS1}} \tag{10.22}$$

For balanced 50/50 couplers:

$$U_{\text{BS}} = \frac{1}{\sqrt{2}} \begin{pmatrix} 1 & i \\ i & 1 \end{pmatrix} \tag{10.23}$$

Step 2: Compute coincidence rate

```python
@jit
def sensor_coincidence(phi, splitting_ratio=0.5):
    """
    WALTHER: Compute coincidence rate vs phase for HOM sensor.

    Args:
        phi: Phase difference between arms [rad]
        splitting_ratio: Coupler splitting (0.5 = 50/50)

    Returns:
        P_coinc: Coincidence probability
    """
    theta = jnp.arccos(jnp.sqrt(splitting_ratio))

    # Transfer through interferometer
    # |1,1> input -> measure coincidence at outputs
    amp_11 = jnp.cos(theta)**2 - jnp.sin(theta)**2 * jnp.exp(1j*phi)
    amp_20 = jnp.sqrt(2) * jnp.cos(theta) * jnp.sin(theta) * (1 +
        jnp.exp(1j*phi))

    P_coinc = 0.5 * (1 - jnp.cos(phi))  # Simplified for 50/50
    return P_coinc

# Sensitivity: derivative of coincidence rate
@jit
def sensor_sensitivity(phi):
    """Phase sensitivity dP/dphi at operating point."""
    return 0.5 * jnp.sin(phi)
```

Listing 8: HOM sensor forward analysis.

Step 3: Determine operating point

Maximum sensitivity occurs at $\phi = \pi/2$:

$$\left.\frac{dP_{\text{coinc}}}{d\phi}\right|_{\phi=\pi/2} = 0.5 \tag{10.24}$$

For 1 nm resolution at $\lambda = 1550$ nm with $n = 1.5$:

$$\delta\phi = \frac{2\pi n}{\lambda}\delta x = \frac{2\pi \times 1.5}{1550 \text{ nm}} \times 1 \text{ nm} = 6.1 \text{ mrad} \tag{10.25}$$

10.9.4 Matsui-Nariai Design: Inverse Optimization

Step 4: Optimize coupler design

The target is 50/50 splitting with maximum tolerance:

```python
@jit
def coupler_loss(params, target_ratio=0.5):
    """
    MATSUI-NARIAI: Optimize coupler for target splitting ratio.

    Args:
        params: [kappa, L] - coupling coefficient and length
        target_ratio: Target power splitting ratio

    Returns:
        loss: Squared error from target
    """
    kappa, L = params
    theta = kappa * L  # Coupling angle
    ratio = jnp.sin(theta)**2
    return (ratio - target_ratio)**2

# Optimize for 50/50 with maximum tolerance
from jax.scipy.optimize import minimize

result = minimize(
    coupler_loss,
    x0=jnp.array([0.5, 3.14]),  # Initial guess
    method='BFGS'
)
kappa_opt, L_opt = result.x
print(f"Optimal: kappa = {kappa_opt:.3f} mm^-1, L = {L_opt:.3f} mm")
```

Listing 9: HOM sensor coupler optimization.

Step 5: Extract tolerances via Hessian

```python
# Hessian at optimal point
H = hessian(coupler_loss)(jnp.array([kappa_opt, L_opt]))

# Eigenvalue decomposition for tolerance ellipse
eigvals, eigvecs = jnp.linalg.eigh(H)

# Tolerance for 1% splitting ratio error
delta_r_max = 0.01  # 1% from 50/50
tolerances = jnp.sqrt(2 * delta_r_max / eigvals)

print(f"Coupling tolerance: +/- {tolerances[0]/kappa_opt*100:.2f}%")
print(f"Length tolerance: +/- {tolerances[1]*1000:.1f} um")
```

Listing 10: HOM sensor tolerance analysis.

10.9.5 Final Sensor Specifications

Table 10.9: HOM Sensor Final Specifications

Parameter	**Nominal**	**Tolerance**	**Notes**
Coupler splitting	50:50	±1%	Defines sensitivity
Coupling coefficient	0.393 mm^{-1}	±2%	SiN platform
Coupler length	4.0 mm	±20 μm	Photolithography
Sensing arm length	5.0 mm	±100 nm	Phase stability
Propagation loss	< 0.05 dB/cm	Max	SiN requirement
HOM visibility	$> 98\%$	Min	Photon quality
Performance Metrics			
Displacement resolution	1 nm		At optimal ϕ
Dynamic range	100 μm		Full fringe counting
Update rate	10 kHz		Coincidence rate limited

The HOM sensor design demonstrates the advanced capabilities of the DEE framework for quantum photonics. The Hessian-QFI connection ensures that designs optimized for manufacturing tolerance automatically achieve good quantum sensing performance. The specification sheet provides a complete fabrication target for foundry submission.

10.10 Production Relevance: From Lab to Fab

Transitioning quantum walk devices from research demonstrations to manufacturable products requires addressing fabrication platforms, yield analysis, and integration challenges. This section provides practical guidance for the optical engineer facing production decisions.

10.10.1 Fabrication Platforms

Table 10.10 compares current fabrication options:

Table 10.10: Waveguide Array Fabrication Platforms

Platform	**Loss [dB/cm]**	**Coupling Control**	**Quantum Suitability**	**Volume Cost**
Femtosecond laser	0.2	±5%	Good (research)	High
Silicon photonics (SOI)	2.0	±1%	Fair (high loss)	Low
Silicon nitride	0.1	±2%	Excellent	Medium
Lithium niobate	0.5	±3%	Good (with SPDC)	High
Silica PLC	0.05	±2%	Excellent	Medium

Recommendation: For quantum applications requiring $\mathcal{F} > 0.95$, silicon nitride or silica PLC are the preferred platforms. Silicon photonics is suitable only for short devices ($L < 2$ mm) due to propagation loss.

10.10.2 Yield Analysis

For quantum devices, yield is dominated by the tightest tolerance. With coupling uniformity requirement $\pm 0.5\%$ and typical fabrication variation $\sigma = 2\%$:

$$Y = \prod_{j=1}^{N-1} \text{erf}\left(\frac{\Delta\kappa_{\max}}{\sqrt{2}\sigma}\right) = [\text{erf}(0.18)]^{15} \approx 0.02 \tag{10.26}$$

This 2% yield is economically challenging. Solutions include:

- **Active trimming:** Post-fabrication tuning via heaters or UV exposure
- **Redundant designs:** Multiple arrays per chip with selection
- **Adaptive protocols:** Algorithms that work with imperfect devices
- **Relaxed specifications:** Trade performance for yield

10.10.3 Integration with SPDC Sources

Complete quantum photonic systems require entangled photon sources. Integration options range from hybrid (external sources) to fully monolithic:

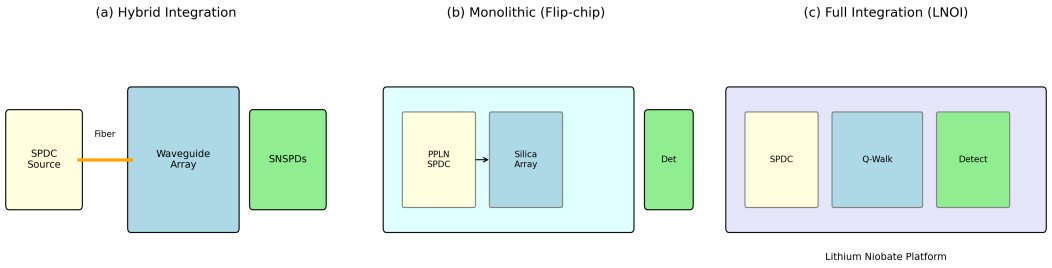

Figure 10.6: Integration architectures for quantum walk chips. (a) Hybrid: External SPDC source fiber-coupled to waveguide array. Simplest approach with best source performance but coupling losses. (b) Monolithic: PPLN waveguide source integrated with silica array via flip-chip bonding. Reduced coupling loss, increased complexity. (c) Full integration: On-chip SPDC, quantum walk, and detection in lithium niobate. Maximum integration, still research-stage.

Production of quantum walk devices is technically feasible with current foundry capabilities, but requires careful platform selection and tolerance management. The DEE framework provides the quantitative tools for making these engineering decisions with confidence.

10.11 Summary

Key Points

1. **Quantum walks spread ballistically** ($\sigma \sim z$) vs. classical diffusive spreading ($\sigma \sim \sqrt{z}$), providing fundamental transport speedup and the characteristic bimodal output distribution.

2. **The eikonal bridge applies directly:** Eigenvalues β_k of the coupling matrix are the eikonals for each supermode; the phase accumulated is $\phi_k = \beta_k z$. The same mathematical framework from Chapter 5 applies—only the observables change.

3. **Two-photon correlations** (bunching/anti-bunching) are purely quantum signatures with no classical analog. The HOM effect is the experimental cornerstone for verifying quantum behavior.

4. **Specification tightening is systematic:** Quantum applications require 10–100× tighter tolerances than classical equivalents, with coupling uniformity the most critical parameter.

5. **The Hessian-QFI connection** enables unified treatment: DEE tolerance analysis directly predicts quantum sensing performance through $F_Q = 4H_{\text{fidelity}}$.

6. **Three dominant failure modes** must be controlled simultaneously: photon distinguishability, optical loss, and fabrication disorder. Each has distinct signatures and mitigation strategies.

7. **Complete design workflows** demonstrated: QRNG (uniform output) and HOM sensor (displacement measurement) follow the W/MN pattern from initialization through specification.

8. **Production is feasible** with silicon nitride or silica PLC platforms, but yield challenges require active trimming or adaptive protocols for tight tolerance requirements.

10.12 Key Equations

Table 10.11: Key Equations for Chapter 10

Eq.	Expression	Name	Reference
(10.3)	$\sigma_{\text{cl}} \propto \sqrt{N}$	Classical spreading	Diffusion
(10.5)	$\sigma_{\text{qu}} \propto z$	Quantum spreading	Ballistic
(10.11)	$\phi_k = \beta_k z$	Eikonal bridge	Central identity
(10.9)	$\beta_k = \beta_0 + 2\kappa\cos(k\pi/(N+1))$	Eigenvalue spectrum	Band structure
(10.13)	$P_{\text{coinc}} = (1-V)/2$	HOM coincidence	Two-photon
(10.16)	$F_Q = 4H_{\text{fidelity}}$	Hessian-QFI	Sensing limit
(10.19)	$\mathcal{F} = e^{-0.115\alpha L}$	Loss fidelity	11% rule

10.13 Specification Translation: Classical to Quantum

Specification Translation

Translation Protocol: When converting a classical waveguide coupler design for quantum applications, apply the following systematic tightening factors:

Table 10.12: Classical to Quantum Specification Translation for Waveguide Arrays

Parameter	**Classical**	**Quantum**	**Factor**	**Limiting Physics**
Waveguide Properties				
Coupling uniformity	$\pm 5\%$	$\pm 0.5\%$	$10\times$	Interference visibility
Propagation loss	1 dB/cm	0.1 dB/cm	$10\times$	Fidelity preservation
Birefringence	10^{-4}	10^{-6}	$100\times$	Polarization purity
Mode field diameter	$\pm 10\%$	$\pm 1\%$	$10\times$	Mode overlap
Dimensional Tolerances				
Waveguide width	± 50 nm	± 5 nm	$10\times$	Effective index
Waveguide spacing	± 100 nm	± 10 nm	$10\times$	Coupling coefficient
Device length	± 50 μm	± 5 μm	$10\times$	Phase accumulation
Environmental				
Temperature stability	± 1 K	± 0.1 K	$10\times$	Index drift
Vibration isolation	Commercial	Research	—	Phase noise
Interface				
Fiber coupling loss	1 dB	0.1 dB	$10\times$	Photon budget
Facet reflectivity	$< 1\%$	$< 0.01\%$	$100\times$	Interference artifacts

10.14 Problems

10.14.1 Walther Problems (Forward Analysis)

Problem 10.1W

A 21-waveguide array has uniform coupling $\kappa = 1.0$ mm^{-1}. A single photon is injected into the center waveguide.

(a) Calculate the eigenvalue spectrum $\{\beta_k\}$ using Eq. (10.9).

(b) Simulate the quantum walk for $L = 5$ mm and plot the output probability distribution.

(c) Calculate the spreading width σ and compare to the classical prediction $\sigma_{\text{cl}} = \sqrt{2\kappa L}$.

(d) At what length does the quantum walk reach the array boundaries?

Solution Hints 10.1W

(a) Use $\beta_k = 2\kappa \cos(k\pi/22)$ for $k = 1, \ldots, 21$. Bandwidth $= 4\kappa = 4$ mm^{-1}.

(b) Decompose initial state into eigenmodes, propagate with phases $e^{-i\beta_k L}$, extract $|c_j|^2$.

(c) Quantum: $\sigma_Q \approx \kappa L = 5$ waveguides. Classical: $\sigma_{\text{cl}} = \sqrt{10} \approx 3.2$. Ratio ≈ 1.6.

(d) Boundary reached when $\sigma_Q \approx N/2 = 10.5$, so $L \approx 10.5$ mm.

Problem 10.2W

Two indistinguishable photons are injected into waveguides $j = 9$ and $k = 13$ of a 21-waveguide array.

(a) Write the input state in second-quantization notation.

(b) Compute the two-photon correlation matrix $\Gamma_{mn}(L)$ for $L = 5$ mm.

(c) Identify waveguide pairs (m, n) showing bunching ($\Gamma_{mn} > \Gamma_{\text{classical}}$).

(d) What is the probability of detecting both photons in the same waveguide?

Solution Hints 10.2W

(a) $|\psi_{\text{in}}\rangle = \hat{a}_9^\dagger \hat{a}_{13}^\dagger |0\rangle$.

(b) Use Eq. (10.15) with unitary $U = e^{-i\mathbf{C}L}$.

(c) Bunching occurs at array center; anti-bunching at edges.

(d) Sum diagonal elements: $P_{\text{same}} = \sum_m \Gamma_{mm}$.

10.14.2 Matsui-Nariai Problems (Inverse Design)

Problem 10.1MN

Design a waveguide array that produces a uniform output distribution $P_j = 1/N$ for single-photon input.

(a) For $N = 8$ waveguides, determine the minimum κL product required.

(b) Using JAX optimization, find optimal coupling perturbations $\delta\kappa_j$.

(c) Calculate manufacturing tolerances for $\mathcal{F} > 0.99$.

(d) Compare your design to a classical power splitter (tree of 50/50 couplers).

Solution Hints 10.1MN

(a) Minimum $\kappa L \approx \pi$ for full spreading; optimize around $\kappa L = 4$.

(b) Use `optimize_array()` from Listing 2.

(c) Extract tolerances from Hessian eigenvalues per Listing 4.

(d) Classical 1:8 splitter uses tree of 50/50 couplers; quantum design is more compact but requires tighter tolerances.

Problem 10.2MN

Design an array that maximizes HOM visibility for photons input at waveguides 1 and N.

(a) What is the theoretical maximum visibility for a uniform array?

(b) Optimize coupling coefficients to achieve $V > 0.99$.

(c) How does the optimal design depend on array length L?

(d) Specify tolerance on κ uniformity for $V > 0.95$.

Solution Hints 10.2MN

(a) For uniform array with symmetric input, $V_{\max} = 1$ at specific lengths.

(b) Use `hom_grad` for gradient-based optimization.

(c) Optimal κL values are periodic; first maximum near $\pi/2$.

(d) Compute $\partial V/\partial\kappa$ and invert for tolerance.

10.14.3 Quantum Extension Problems

Problem 10.1Q

Analyze the quantum sensing capability of a 16-waveguide array optimized for uniform output.

(a) Compute the Quantum Fisher Information F_Q for phase estimation.

(b) What is the minimum detectable phase shift with $N = 10^6$ photons?

(c) Compare to the SQL and Heisenberg limits.

(d) How does F_Q scale with array size?

Solution Hints 10.1Q

(a) Use $F_Q = 4H_{\text{fidelity}}$ from DEE tolerance analysis.

(b) $\delta\phi_{\min} = 1/\sqrt{N \cdot F_Q}$.

(c) SQL: $\delta\phi = 1/\sqrt{N}$; Heisenberg: $\delta\phi = 1/N$. Quantum walk typically achieves intermediate scaling.

(d) F_Q scales approximately linearly with N for optimized arrays.

References

[1] W. Feller, *An Introduction to Probability Theory and Its Applications*, Vol. 1, 3rd ed. (Wiley, 1968).

[2] Y. Aharonov, L. Davidovich, and N. Zagury, "Quantum random walks," *Phys. Rev. A* **48**, 1687 (1993).

[3] J. Kempe, "Quantum random walks: An introductory overview," *Contemp. Phys.* **44**, 307 (2003).

[4] D. N. Christodoulides, F. Lederer, and Y. Silberberg, "Discretizing light behaviour in linear and nonlinear waveguide lattices," *Nature* **424**, 817 (2003).

[5] C. K. Hong, Z. Y. Ou, and L. Mandel, "Measurement of subpicosecond time intervals between two photons by interference," *Phys. Rev. Lett.* **59**, 2044 (1987).

[6] R. Loudon, *The Quantum Theory of Light*, 3rd ed. (Oxford University Press, 2000).

[7] A. Politi, M. J. Cryan, J. G. Rarity, S. Yu, and J. L. O'Brien, "Silica-on-silicon waveguide quantum circuits," *Science* **320**, 646 (2008).

[8] A. Peruzzo *et al.*, "Quantum walks of correlated photons," *Science* **329**, 1500 (2010).

[9] Y. Bromberg, Y. Lahini, R. Morandotti, and Y. Silberberg, "Quantum and classical correlations in waveguide lattices," *Phys. Rev. Lett.* **102**, 253904 (2009).

[10] A. Crespi *et al.*, "Anderson localization of entangled photons in an integrated quantum walk," *Nature Photon.* **7**, 322 (2013).

[11] N. C. Harris *et al.*, "Quantum transport simulations in a programmable nanophotonic processor," *Nature Photon.* **11**, 447 (2017).

[12] J. Wang, F. Sciarrino, A. Laing, and M. G. Thompson, "Integrated photonic quantum technologies," *Nature Photon.* **14**, 273 (2020).

[13] J. Carolan *et al.*, "Universal linear optics," *Science* **349**, 711 (2015).

[14] J. B. Spring *et al.*, "Boson sampling on a photonic chip," *Science* **339**, 798 (2013).